Development of Direct Tension Test Method for Ultra-High-Performance Fiber-Reinforced Concrete

by Benjamin A. Graybeal and Florent Baby

Sustained postcracking tensile resistance is a fundamental mechanical characteristic of ultra-high-performance fiber-reinforced concrete (UHPFRC). This research program developed a simple, reliable direct tension test (DTT) method that can generate the uniaxial tensile mechanical response for both cast and extracted UHPFRC samples. The developed test method emulates DTT methods already commonly used in the mechanical testing of metals, thus addressing many of the hurdles that can hinder the implementation of new test methods. It was demonstrated to be applicable to two UHPFRCs with two different steel fiber reinforcement contents in seven total sets of specimens. The test method can facilitate the development of appropriate quality control processes for UHPFRC, the advancement of UHPFRC mixture designs, and the development of strain-based UHPFRC structural design criteria.

Keywords: direct tension test; tensile stress-strain response; ultra-high-performance fiber-reinforced concrete.

INTRODUCTION

Ultra-high-performance fiber-reinforced concrete (UHPFRC) is a class of cementitious composite materials designed to exhibit exceptional mechanical and durability properties, including sustained postcracking tensile strength.[1-9] Laboratory tests of structural elements have clearly indicated that UHPFRC components can exhibit tensile mechanical properties far in excess of those expected from conventional and fiber-reinforced concretes.[10-16] However, specific quantification of these tensile mechanical properties has proven difficult, leading to hesitancy among designers considering the engagement of these properties in UHPFRC components within the civil infrastructure.

Small-scale tests are commonly applied when there is a desire to quantify specific aspects of the mechanical performance of a structural material. For concrete, compressive strength is a critical property; thus, direct uniaxial compression tests, such as ASTM C39/C39M,[17] are commonly applied as a means of performance assessment. Test methods for structural materials more commonly associated with tensile behaviors have also become standardized to the point of widespread acceptance. For structural steel, ASTM E8/E8M[18] provides direction for various mechanical tests, including a uniaxial direct tension test (DTT) on a rectangular piece of steel plate. Simple tests such as these are widely engaged because they provide a direct indication of the desired result and can be completed with standardized testing equipment.

Due to its comparatively small tensile stress and strain capacities, conventional concrete does not lend itself to the application of DTT methods. For fiber-reinforced concretes, tension test methods have included both direct and indirect assessments, including some that have been standardized.[4,19,20] However, in all cases, the test methods have fundamental shortcomings that limit their applicability. Common

concerns with flexure-type indirect test methods include the strain gradient allowing for restraint of the most heavily loaded tensile face, the assumptions and complex computations necessary to back-calculate the uniaxial behavior, and the complex multiple cracking behaviors that occur in a notched specimen.[21,22]

Direct-tension-type tests alleviate many of these concerns but encounter hurdles as well. Although the internal stress state, the measurement of strain, and the computation of results are straightforward with DTTs, developed methods have tended to require specialized testing equipment and, in many cases, custom-fabricated specimens.

The research discussed herein focuses on developing a practical test method for the direct assessment of UHPFRC tensile properties, thus facilitating the development of a standardized quality assurance test program that could be applied to UHPFRC structural elements. Through this test method, a pair of commercially available UHPFRC-type materials was assessed. The DTT results support a UHPFRC mechanical tensile response model and a methodology for developing statistical-based stress-strain relationships for use in structural design of UHPFRC components.

RESEARCH SIGNIFICANCE

Appropriate, efficient use of UHPFRC requires a thorough understanding of the tensile mechanical behaviors from the elastic straining of the composite matrix through strain localization at a discrete crack. This paper presents a new test method loosely based on test methods commonly applied to the tensile testing of metals. This tension test method uses commercially available testing equipment, can be applied to cast or cut specimens, and does not require significant interpretation or adaptation of results. As such, the test method can foster the development of UHPFRC materials, as well as facilitate the quality control and assessment of UHPFRC structural elements.

BACKGROUND

Direct tensile testing of concrete dates back to at least 1928, when Gonnerman and Shuman[23] tested 152 mm (6 in.) diameter conventional concrete cylinders by gripping the specimen ends with cylindrical steel straps friction-clamped to the concrete circumference. In the intervening years, DTT method development for concrete has progressed along two parallel paths. One path can be generally described as test

Benjamin A. Graybeal *leads the Structural Concrete Research Program for the Federal Highway Administration at the Turner-Fairbank Highway Research Center in McLean, VA. He received his BS and MS from Lehigh University, Bethlehem, PA, and his PhD from the University of Maryland, College Park, MD. His research interests include structural application of advanced cementitious materials, concrete material characterization, experimental evaluation of highway bridge structures, and nondestructive evaluation techniques.*

Florent Baby *is a Researcher in the Bridges and Structures Department at Institut français des sciences et technologies des transports, de l'aménagement et des réseaux (IFSTTAR) (formerly the French Central Laboratory of Roads and Bridges [LCPC]). He graduated from École Nationale des Travaux Publics de l'Etat and Master MEGA, Lyon, France. His research interests include the behavior of structures made of ultra-high-performance fiber-reinforced concrete and advanced cementitious materials characterization.*

methods that use adhesives to affix the end surfaces of a tensile specimen to testing machine fixturing, after which a uniaxial tensile load is applied. Examples include both standardized[24,25] and nonstandardized[5,26-32] test methods. A significant benefit of this type of test is that the specimen can be loaded in uniaxial tension without the imposition of significant bending stresses. However, such a test requires the specimen to be glued between the crossheads of the test machine, thus significantly increasing the duration of any individual test. Moreover, local stress effects in a specimen near the adhered surfaces frequently result in premature, nonuniform specimen failure.

The second type of DTTs can broadly be classified as test methods that grip parallel sides at each end of the concrete specimen. Prior work along this path has tended toward the use of custom-fabricated dogbone-shaped specimens,[33-41] but some work on prismatic specimens has been completed as well.[42-45] Although tests requiring custom fabrication can relate valuable results, this type of test has inherent limitations, as it is not generally applicable to the types of extracted specimens that would accurately represent the tensile properties of UHPFRC in a structural element. Some of these test methods[33,34,42,44] allow for relative rotation of the ends of a specimen, thus reducing initial bending while invalidating the postcracking response, which is central to the behavior of UHPFRC. Others[31,42,43] notch the specimen at midspan, thus predetermining the failure location while simultaneously imparting a stress concentration.

EXPERIMENTAL INVESTIGATION

The experimental investigation focused on developing and demonstrating a practical DTT for UHPFRC. The requirements set forth in the test development included the following:

- The test method must accurately capture the uniaxial tensile mechanical response of UHPFRC from elastic behavior through strain localization at a single crack;
- The test method must strive to limit the magnitude of flexural strain in the test specimen, thus limiting the strain gradient and reducing flexure-induced local restraint at strain discontinuities (that is, cracks);
- The test method must forestall the relative rotation of the specimen ends so as to limit the nonuniform localization of strain within individual cracks;
- The test method must be able to be completed using commercially available testing equipment;
- The test method must be applicable to both cast and extracted specimens without requiring the use of milling or machining of specimens; and
- The test method must be able to be completed in a sufficiently short time frame that a set of at least six speci-

mens from a particular batch could be tested in less than 8 hours.

The existing standardized test method for tensile mechanical assessment of a rectangular steel plate, as defined in ASTM E8/E8M[18]—commonly referred to as the "dogbone test"—was engaged as a starting point in the development of this test method. Because ASTM E8/E8M[18] is frequently used by steel producers and commercial mechanical testing firms to verify structural steel tensile behavior, the equipment necessary for the completion of this test is commercially available. This test method suggests that the test specimen consists of a nominally prismatic shape with larger end blocks tapering to a constant cross section within the instrumented length. The ends of the steel specimen are gripped within the test frame to eliminate any relative end rotation and ensure that uniaxial stresses are generated in the specimen. The uniaxial tensile strain is measured by an extensometer attached to the specimen over the constant cross-section gauge length. The specimen is loaded by applying a constant displacement to one crosshead relative to the other. The test concludes once the full range of tensile behaviors, including tensile rupture, has been recorded.

Modifications were necessary to adapt this test method for application to UHPFRC. First, the shape of the test specimen was modified. The casting or extracting of prismatic UHPFRC specimens is feasible, while the machining of such specimens into a tapered shape is problematic. To increase the likelihood of specimen failure within the instrumented gauge length, tapered aluminum plates were affixed with epoxy on two sides of each end of the specimen. A high-strength, high-modulus, structural-grade epoxy was selected, as this allowed for stiffness compatibility between the UHPFRC, the adhesive, and the aluminum. Second, the common method of measuring strain in a steel specimen was modified so as to allow for the capture of any nonuniform strains applied to the concrete. The strain was captured with a parallel ring extensometer similar in concept to the parallel ring compressometer sometimes used in the testing of concrete cylinders for modulus of elasticity. The extensometer contained four linear variable differential transformers (LVDTs).

An illustration of the specimen shape and gripping setup is shown in Fig. 1. The limit of the hydraulic wedge grip mouth opening led to the selection of a prismatic specimen with a 50.8 mm (2 in.) square cross section for all tests. The tapered aluminum plates affixed to two sides of each end of each specimen were nominally 4.76 mm (0.188 in.) thick and linearly tapered to 1.0 mm (0.04 in.) thick over a 50.8 mm (2 in.) length. Two different specimen lengths, with corresponding changes in instrumented gauge lengths, aluminum plate dimensions, and grip lengths, were tested within the program. "Long" refers to a 431.8 mm (17 in.) total length prism, while "short" refers to a 304.8 mm (12 in.) total length prism. In all cases, the specimens were single-point cast in prismatic molds, allowing the UHPFRC to flow along the length of the form.

Figure 2 shows a 431.8 mm (17 in.) long specimen in the test machine under load. The hydraulic-actuated, computer-controlled load frame includes variable pressure hydraulic wedge grips. Tests were completed under actuator displacement control, while data from the actuator load cell, actuator displacement, and four specimen strain LVDTs were electronically captured. A constant displacement rate of 0.00254 mm/s (0.0001 in./s) was used, and loading was continued until either a gauge length strain of 25,000 µε was
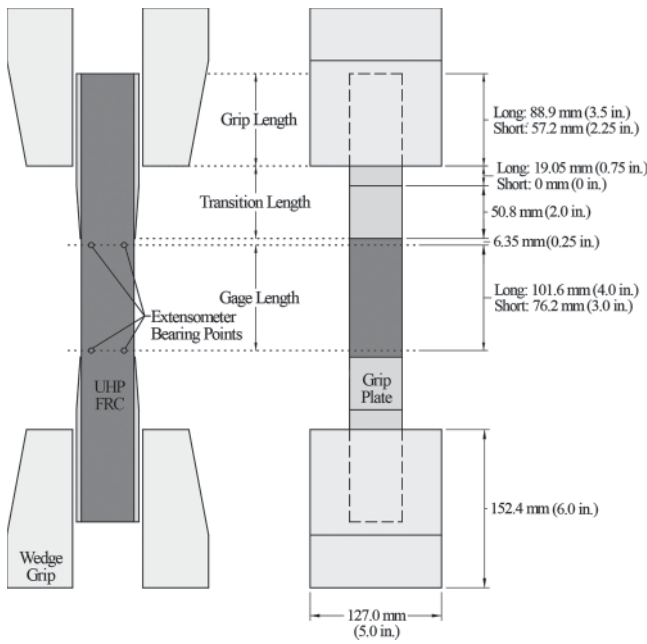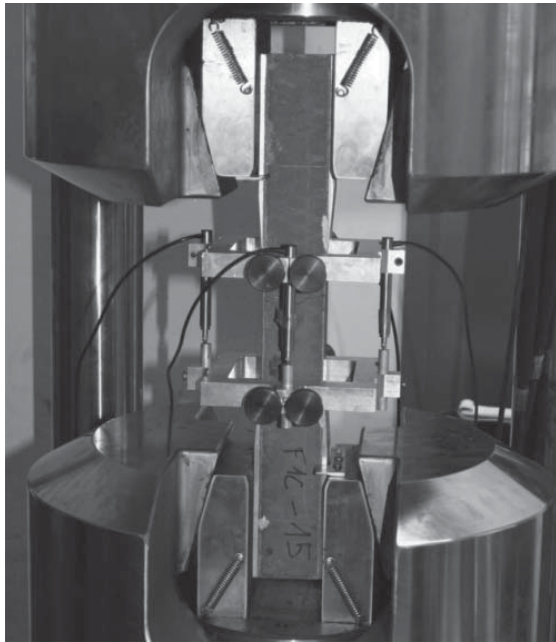
Fig. 1—DTT specimen.
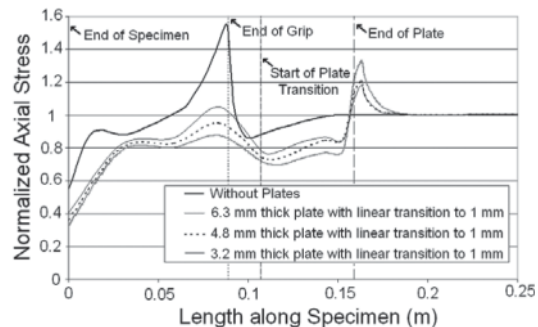

Fig. 2—Testing of 431.8 mm (17 in.) long specimen.

achieved or the specimen had localized at a crack outside of the gauge length.

TEST PROGRAM

The test program included both a development phase and an execution phase. In the development phase, a series of physical and analytical tests were completed to assess the impact of a variety of grip-plate configurations on the performance of a specimen during a test. The analytical modeling was completed through the use of finite element modeling software. The UHPFRC and aluminum plates were modeled under the assumptions of linear elastic behavior with perfect bond between the UHPFRC and the plates, and the moduli of elasticity were assumed to be 55 and 70 GPa (7980 and 10,150 ksi), respectively. A variety of aluminum grip-plate thicknesses and transition geometries were considered to minimize the magnitude of the stress disturbance within the prismatic portion of the UHPFRC test specimen. Through this numerical study, the results of which are shown in Fig. 3, the grip-plate geometry was optimized to minimize stress disturbance while also allowing for simplified plate fabrication and attachment. For the chosen grip-plate configuration, the idealized local stress at the termination of the grip plate is less than 20% greater than the uniaxial tensile stress field at the center of the specimen, and the imperfect epoxy bond will result in further reduction in practice. This can be compared to a 60% increase in local uniaxial stress if the transition plates were not present. The chosen plate configuration also reduces the length of the stress disturbance to a small zone near the tip of the plate termination. Precursor physical tests verified that the chosen plate geometry met or surpassed the performance of the alternates shown in Fig. 3.

The execution phase of this program included the completion of DTTs and other associated tests on four sets of UHPFRC specimens. Testing included the DTT developed herein along with four-point flexure tests and compression behavior mechanical performance tests completed on the same UHPFRCs. The flexure test results are reported elsewhere.[46,47]

Table 1 provides details on the four sets of specimens, including which tests were completed on each set. The first character of the specimen name indicates the type of UHPFRC material used and the second character indicates the type of post-cast curing regime applied. A "1" indicates that the specimen set was subjected to steam treatment curing at 90°C (194°F) and 95% humidity for 48 hours, while a "2" indicates that the specimen set was held in a standard labora-

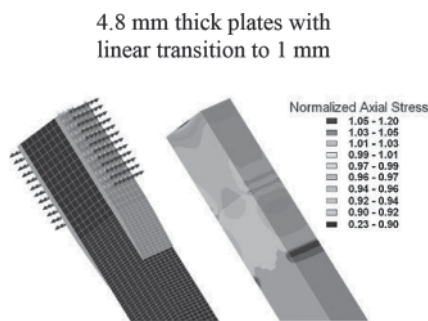*Fig. 3—Finite element modeling of grip-plate geometry and local axial stresses on surface of UHPFRC prism. (Note: 1 mm = 0.0394 in.)*

Table 1—Sets of test specimens and UHPFRC material properties

Group	UHPFRC	Steel fiber volumetric percentage	Curing regime	DTT— short	DTT— long	Four-point flexure	Density, kg/m³ (lb/ft³)	Compressive strength, MPa (ksi)	Modulus of elasticity, GPa (ksi)
F1A	F	2	Steam	X	X	X	2570 (160.4)	220 (32.0)	61.0 (8840)
F2A	F	2	Lab	X	X	X	2545 (158.9)	192 (27.9)	62.8 (9110)
F1C	F	2.5	Steam	X	X	X	2569 (160.4)	212 (30.7)	60.3 (8740)
B2A	B	2.5	Lab	X	—	X	2690 (168.0)	213 (30.9)	63.9 (9270)

Table 2—UHPFRC mixture designs

Material	UHPFRC F-2% amount, kg/m³	UHPFRC F-2.5% amount, kg/m³	UHPFRC B amount, kg/m³
Premix*	2195	2161	2296
High-range water-reducing admixture	30	29	50
13 mm steel fibers	156	195	0
20 mm steel fibers	0	0	195
Water	130	128	190

*Proprietary mixture designs, including inert and cementitious constituents.
Notes: 1 kg/m³ = 0.062 lb/ft³; 1 mm = 0.0394 in.

tory environment prior to the test. Steam treatment, which accelerates the attainment of desirable material characteristics, is sometimes specified for prefabricated UHPFRC components.[32] All specimens in a particular set were cast from an individual batch of UHPFRC.

UHPFRC MIXTURE DESIGNS AND MATERIAL PROPERTIES

Three UHPFRC mixture designs were engaged in this study and are provided in Table 2. The UHPFRC F mixture designs are effectively the same, aside from the two different volumetric percentages of fiber reinforcement. This particular UHPFRC is a proprietary product that is commercially available in North America and other parts of the world. UHPFRC B is a different proprietary product that is only commercially available in parts of Western Europe. Straight, nondeformed steel fiber reinforcement was used in all specimens. The UHPFRC F specimens used fibers 13 mm (0.5 in.) long and 0.2 mm (0.008 in.) in diameter. The UHPFRC B specimens used fibers 20 mm (0.8 in.) long and 0.3 mm (0.012 in.) in diameter. As is common in UHPFRC structural components, the specimen cross-sectional dimensions and implemented casting method resulted in the fibers inherently displaying a nonuniform orientation throughout the gauge length of each specimen. Each UHPFRC was mixed and cast on its native continent, and all mechanical tests were completed at the U.S. Federal Highway Administration's Turner-Fairbank Highway Research Center in McLean, VA.

As a group, the four sets of UHPFRC materials tested in this study can generally be described as high-compressive-strength, high-stiffness, steel fiber-reinforced cementitious composite materials. The density, compressive strength, and compressive modulus of elasticity for each set of specimens are provided in Table 1. All of these values were calculated from tests on cast cylinders, with cylinders with a diameter of 76 and 110 mm (3 and 4.33 in.) used for UHPFRC F and B, respectively. Cylinder lengths were approximately twice their diameters. Aside from minor modifications frequently employed in the compression testing of UHPFRC, the modulus and strength tests were completed according to ASTM C469/C469M[48] and ASTM C39/C39M,[17] respectively. These modifications included an increased loading rate (1 MPa/s

[150 psi/s]), the use of a three-LVDT parallel ring compressometer for strain readings, and the loading of each specimen continuously through compression failure.[49] The density readings were captured on the end-ground cylinders immediately before compression testing, with density being calculated as weight divided by cylindrical volume.

TEST RESULTS AND ANALYSIS

Test results from seven sets of specimens were captured through this test program, and 28 of those results are discussed herein. As an example, Fig. 4 shows the response of a specimen from Set B2A. This two-part plot affords both an expanded view of the elastic response through first cracking as well as a global view of the tensile response through 1% strain. To generate the response shown in the figure, the average axial stress f_c was calculated with Eq. (1) and the average axial strain ε_c was calculated with Eq. (2); P is the load, A is the cross-sectional area, and L is the gauge length.

$$f_c = \frac{P}{A} \tag{1}$$

$$\varepsilon_c = \frac{\Delta L}{L} \tag{2}$$

First cracking occurs at a decreased stress level as compared to the plateau stress in the multi-cracking phase. This reduced stress level is attributed to minor bending strains imparted into the specimen during initial gripping in the test machine. Initial cracking relieves the flexural component of these stresses, thus allowing for a generally consistent cementitious matrix cracking threshold through the remainder of the multi-cracking phase. For each specimen, the initial bending stresses and the reduction in bending strains after first cracking was verified through comparison of individual LVDT readings to the average of the four readings. Figure 5 presents the elastic stresses observed during the initial loading—the same specimen whose results are presented in Fig. 4. These elastic stresses were calculated based on the addition of the linear elastic flexural stresses
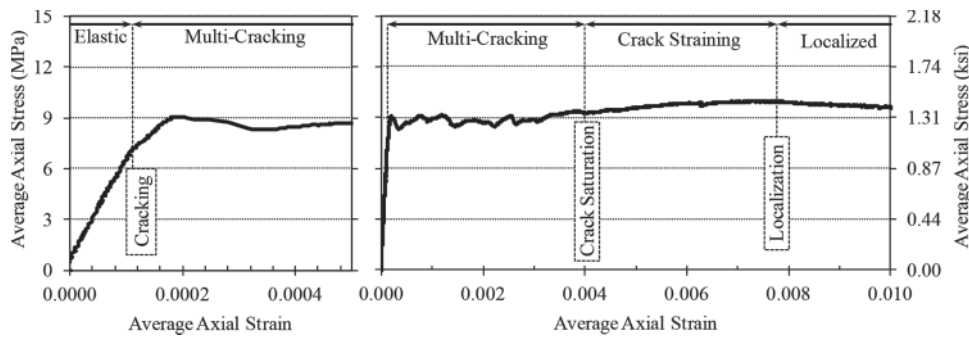
Fig. 4—Uniaxial tensile stress-strain response from specimen in Set B2A.

imparted during gripping and the axial stresses applied after gripping as calculated stresses from Eq. (1). Figure 6 presents the postcracking strain results for the same specimen. Here, the postcracking strain observed on each face is compared directly to the average of the four facial strain values to provide an indication of the uniformity of loading. The strain gradient generated at initial gripping decreases after the first crack occurrence; thus, the nonlinear part of the response obtained with this test method can be considered as the material postcracking behavior under direct tension.

The stress-strain results from all 28 specimens are presented in seven sets within Fig. 7. The number of valid tests completed within each set is shown in a circle in the upper right-hand corner of each plot in Fig. 7. Each set included either five or six nominally identical replicates, thus indicating that a somewhat significant number of test specimens within some sets were discarded. Exclusions of test specimens resulted from misapplication of the test procedure, proportionally large bending stresses applied during gripping, strain localization outside of the gauge length, or the non-strain-hardening response of the specimen. The combined volumetric percentage and efficiency of the fiber reinforcements used in these UHPFRCs produced peak tensile capacities similar to the multi-cracking plateau stress, thus increasing the likelihood of occasionally observing a strain-softening response.

An annotated illustration of the overall tensile response observed in this test program is provided in Fig. 8. This behavior is described in further detail after the presentation of test results.

Elastic regime

Elastic flexural strains imparted into each specimen during the gripping phase were calculated based on the displacements captured by the four LVDTs in the extensometer. The gripping occurred under a computer-controlled, hydraulic-actuated, zero-load condition, and the strains were calculated according to the assumption of linear elastic flexural behavior. As shown in Table 3, for a set of specimens, the average tensile strain on the face of a specimen, as induced by the gripping process, ranged from a low of 0.000034 to a high of 0.000129. Commensurate with the fixed-end gripping of the test specimens and the small, inevitable fixed-end translations of one end of each specimen relative to the other, the gripping-induced strains in the short specimens tended to be 1.5 to 2.0 times larger than the gripping-induced strains in the long specimens. Equation (3) shows the constant moment generated in the specimen by the fixed-end translation. Under the assumption that the translation Δ, the modulus of elasticity E, and the moment of inertia I
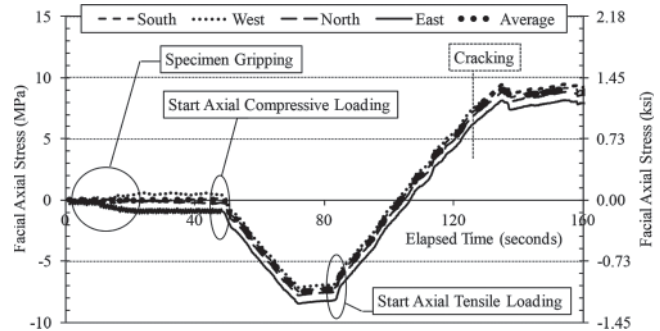

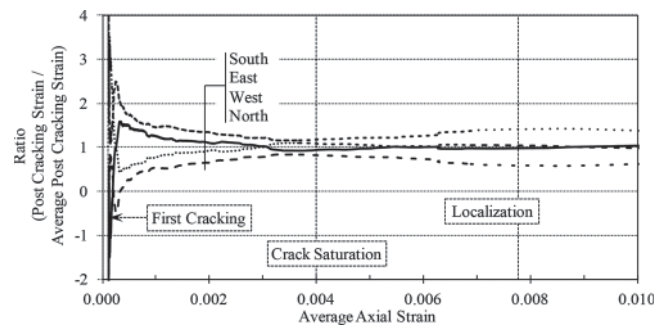*Fig. 5—Elastic facial axial stresses from specimen in Set B2A.*

Fig. 6—Postcracking facial strain disparity from specimen in Set B2A.

remain constant for a square prismatic specimen geometry, the shorter-length specimens can be expected to exhibit a 78% increase in moment and, thus, flexural tensile strain. Note that the elastic strains of a small subset of specimens were verified through data collected from electrical resistance strain gauges applied along the gauge length of the gripped faces.

$$\text{moment} = \frac{6EI\Delta}{L^2} \quad (3)$$

The implemented test method also provides a viable means of capturing the elastic stiffness of UHPFRC. Loading started with the application of uniaxial compressive loads to –10.3 MPa (–1.5 ksi), after which uniaxial tensile loads were applied through failure. Table 3 provides the modulus of elasticity results for the seven sets of tested specimens. These values correspond to a linear best-fit approximation of the stress-strain response between the
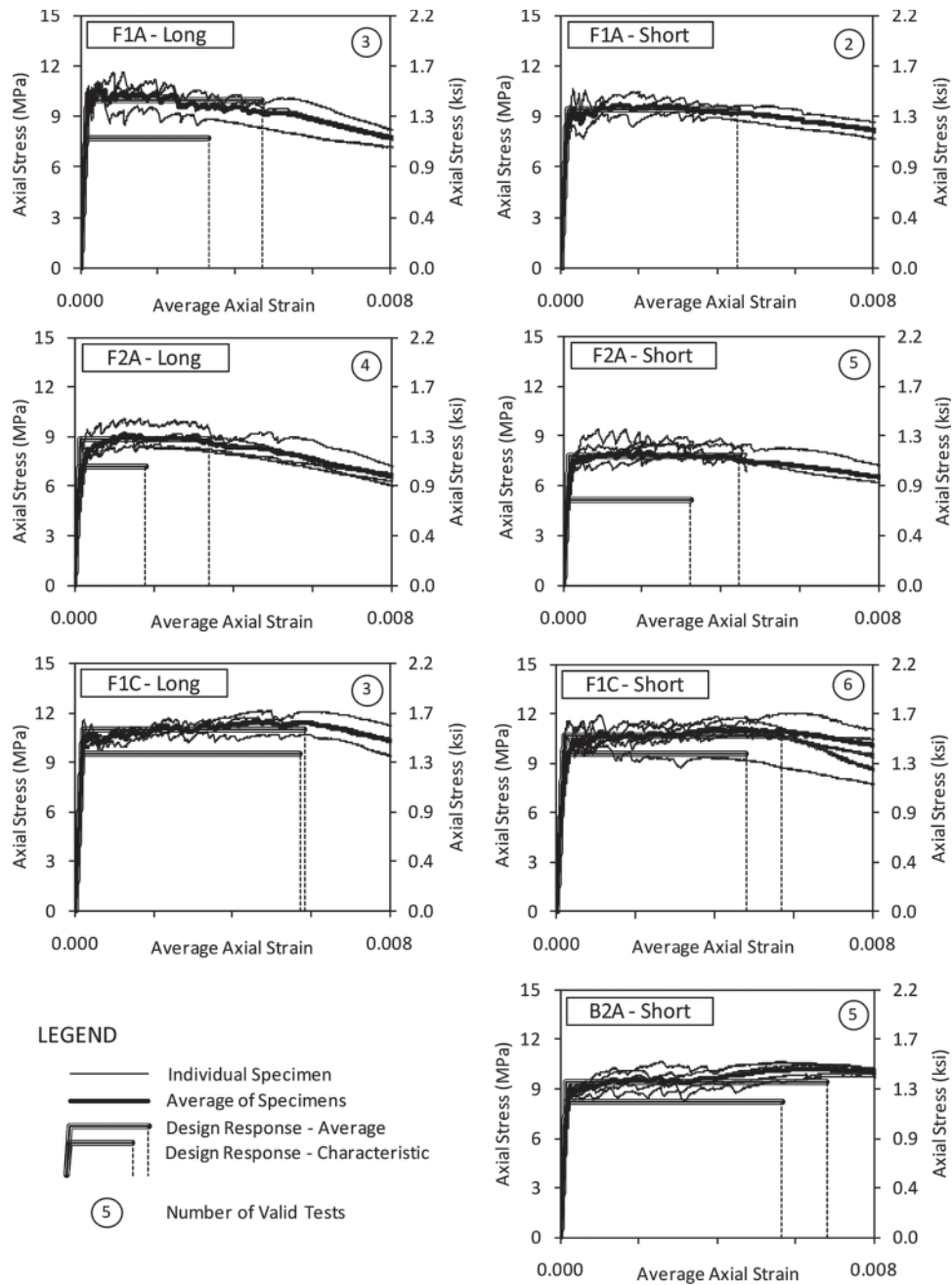
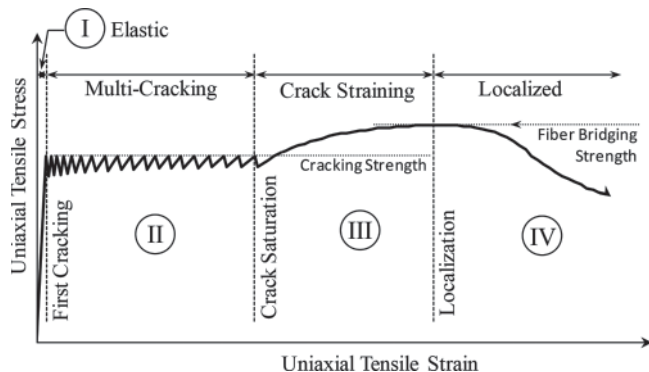Fig. 7—Stress-strain results from seven unique sets of direct tension specimens.

Fig. 8—Idealized uniaxial tensile mechanical response of UHPFRC.

average stresses of –7 and 0 MPa (1.0 and 0.0 ksi) on the tensile branch of the load application. The reported values of approximately 55 GPa (8000 ksi) for UHPFRC F and 62 GPa (9000 ksi) for UHPFRC B are consistent with previously reported modulus of elasticity values for these concretes.[4,49]

Cracking strength

Current practice in the structural design of UHPFRC components frequently relies on an estimation of the tensile cracking strength of the concrete as a defining factor for appropriate limit states.[4] Assessing this property through a test that accurately replicates the type of uniaxial tensile stress state encountered in full-scale components is desirable. The implemented test method provides an appropriate stress state and affords multiple means through which the tensile cracking strength of the UHPFRC matrix can be estimated.

Table 3—DTT mechanical response results

Specimen set	Average flexural tensile strain at gripping	Elastic modulus, GPa	Average first cracking strength, MPa	Facial first cracking strength, MPa	Average multi-cracking stress, MPa	Maximum tensile strength, MPa	Strain at crack saturation	Strain at localization
F1A-Long	0.000069	55.8	9.09	12.83	9.97	11.20	0.004170	0.004720
F1A-Short	0.000126	54.5	8.52	12.05	9.18	10.29	0.005390	0.005920
F2A-Long	0.000067	56.5	6.67	10.08	8.47	9.18	0.003050	0.003410
F2A-Short	0.000082	55.4	5.91	10.25	7.76	8.56	0.003900	0.004760
F1C-Long	0.000034	54.2	9.07	10.34	10.59	11.56	0.005240	0.005842
F1C-Short	0.000055	56.1	8.41	11.09	10.49	11.36	0.004840	0.005685
B2A-Short	0.000129	61.7	6.18	9.29	9.36	10.53	0.004230	0.006480

Note: 1 GPa = 1000 MPa = 145.04 ksi.

The capture of stress-strain data within the implemented test method clearly differentiates elastic behavior from inelastic behavior at the first slope discontinuity in the response. This value, referred to as the "average first cracking strength," is a measure of the average stress on the entire cross section at first cracking. Table 3 provides the average result for each of the seven sets of tested specimens.

The cracking strength of the cementitious matrix can also be assessed through two other measures. First, the aforementioned average first cracking strength can be adjusted to account for the bending stress imparted to the cross section during initial gripping of the specimen. Based on the assumption of elastic behaviors, the facial first cracking strength is calculated by adding the grip-induced flexural tensile component observed at initial gripping to the average first cracking strength. However, although the strain gradient in this test procedure is significantly reduced as compared to that in a flexure test, the cross section at first cracking is still subject to flexural restraint—commonly referred to as a "scale effect"—resulting in a perceived increase in cracking strength.[5,50] Again, Table 3 provides the average result for each of the seven sets of tested specimens.

Alternatively, the entire multi-cracking phase can be engaged to estimate the tensile cracking strength of the cementitious matrix. Because this phase represents a straining of UHPFRC wherein a homogeneous matrix is repeatedly cracked, the average stress during this phase of the response can also provide an indication of the cracking strength. These results are also presented in Table 3. Note that, ideally, the average stress at the crack indications could be averaged; however, practical identification of these individual indications introduces significant qualitative assessment into the process. Therefore, the average stress during the entire multi-cracking phase is used. Note that the magnitude of the stress drop at each crack is dependent on the fiber system (that is, fiber type, modulus of elasticity, bond properties, orientation, and so on), so the level of conservatism induced by using this average cracking stress may vary.[11]

Because the average first cracking stress can underestimate the cracking strength due to grip-induced bending in the specimen and because the facial first cracking strength can overestimate the strength due to the flexural strain gradient, the average stress during multi-cracking is proposed as the most reliable estimate for the UHPFRC matrix cracking strength. This is supported by both the qualitative consistency observed during the multi-cracking phase for specimens in this test program and the standard deviations of the set's cracking strength of results. The average of the standard deviations on each set of results for the average first cracking, facial first cracking, and average multi-cracking results are 1.6, 1.2, and 0.6 MPa (0.24, 0.17, and 0.08 ksi), respectively.

Postcracking tensile regime

The UHPFRC tensile response during the multi-cracking and crack-straining phases can generally be defined through four values: the cracking strength, the maximum tensile strength, the strain at crack saturation, and the strain at localization. Any response after localization represents crack opening and is not discussed herein. The average values from each of the sets of specimens are presented in Table 3. The maximum tensile strength provides an indication of the largest uniaxial stress that can be applied to the UHPFRC prior to the initiation of fiber pullout. The strain at crack saturation indicates the strain at which crack widening begins, potentially impacting durability considerations for the structural component. The strain at localization indicates the strain at which the UHPFRC ceases to display a pseudo-strain response and begins localizing at individual discrete cracks. It must be noted that different UHPFRCs will exhibit different responses depending on the characteristics of the cementitious matrix and the efficiency of the fiber reinforcement. In these tests, UHPFRC B displayed a more distinct crack-straining phase and a larger strain at localization, at least in part due to the preferential longitudinal orientation of the longer fibers. UHPFRC F localized earlier and in closer proximity to the strain at crack saturation.

The overall cracking response of the specimens is shown in Fig. 9. This figure shows a photograph including a single representative sample from each specimen group. Cracking—as identified through evaporative penetrant visual inspection—was marked on the surface of each specimen. These cracks were then traced within the digital photographs to create the figure provided. Dense multiple cracking is apparent in the specimens from the F1C batches, while short specimens from the F1A and F2A batches show more limited multiple cracking.

Average and characteristic tensile mechanical responses

Combining the discrete stress-strain responses from individual specimens provides a robust means of quantitatively assessing the performance of a UHPFRC. For the seven UHPFRC sets tested in this program, the average and standard deviation stresses at strain intervals of 0.000005 were calculated. The average result is plotted as the heavy solid line in each of the plots in Fig. 7. A characteristic curve was
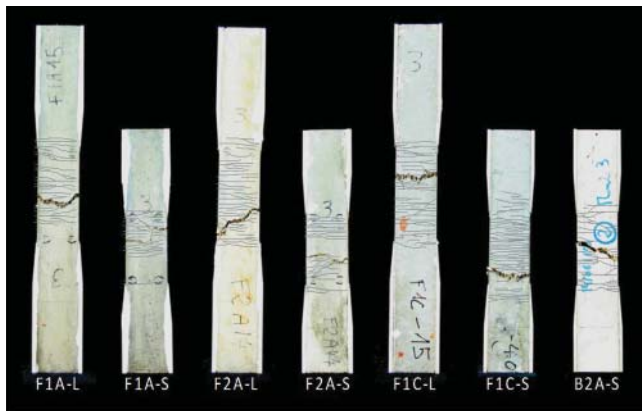
Fig. 9—Cracking present at conclusion of test for representative set of samples.

also calculated for each specimen set, with the stress values reduced from the average stress values by the t-Student coefficient times the standard deviation. The t-Student coefficient is based on the number of valid stress values available at each strain interval. Note that only two acceptable results were obtained for the F1A-Short specimen set, and thus a statistical treatment of the results is not appropriate.

The average design and characteristic design responses were developed for the seven sets of specimens and are shown in Fig. 7. Based on the general behavior of UHPFRC observed herein, an elastic-plastic behavior model with a plateau at a reasonable approximation of the cementitious matrix cracking strength was assumed as a basic response shape. For both the average and characteristic design responses, the elastic portion of the behavior is generated from the average modulus of elasticity of the set of specimens. For the average design response, the plateau resides at the average stress observed in the set of specimens from a strain of 0.0003 through the average crack saturation strain. The value of 0.0003 was chosen, as it is near but always greater than the first cracking strain. This plateau extends from its intersection with the elastic response through the strain at localization. For the characteristic design response, the plateau resides at the average characteristic stress observed within the same range and extends from the elastic response through the characteristic value of the strain at localization. These design responses (and the overall design response concept) provide key information that is critical to the appropriate development of statistically based structural design specifications for UHPFRC.

DISCUSSION
UHPFRC uniaxial tensile response

The typical UHPFRC uniaxial tensile response captured through this test program is illustrated in Fig. 8. This idealized representation includes four distinct phases: I: Elastic; II: Multi-Cracking; III: Crack Straining; and IV: Localized. As their names suggest, these phases refer to specific performance states that occur through the uniaxial straining of the UHPFRC. Phase I, the elastic phase, refers to the global elastic straining of the composite section. This behavior continues through first cracking of the section, which occurs at the tensile strength of the cementitious composite. Phase II, the multiple cracking phase, refers to the portion of the behavior wherein the cementitious matrix repeatedly cracks within the gauge length. Given that the postcracking

strength of each cracked section—as afforded by the steel fiber reinforcement—is greater than the cementitious matrix cracking strength, the specimen tends to accumulate elastic strain in both the uncracked sections of the cementitious matrix between cracks and the fiber reinforcement bridging the cracks but does not experience widening of individual cracks.[51] This phase is characterized by a nearly constant stress level, which is attributed to the homogeneity of the cementitious matrix. The multiple cracking phase is consistent with the experimental results observed in this study and past research—most notably Reference 52. This phase concludes at a point denoted as "crack saturation." Although a small number of additional cracks could occur at the higher stresses generated in the subsequent phase, this point demarcates the change in behavior from deformation dominated by matrix cracking to deformation dominated by straining within existing cracks. Phase III, the crack-straining phase, is the portion of the behavior characterized by increasing crack opening as the fiber reinforcement undergoes a combination of elastic straining and interface debonding. The strain-based phases end when the tensile strength of the strain-hardening composite is reached,[41] referred to herein as the "fiber bridging strength." The final phase, localization, is characterized by the continued widening of an individual crack as the fibers bridging that crack debond and pull out of the matrix. The remainder of the specimen elastically unloads in this phase, meaning that the behaviors in this phase are based on crack opening, not strain.

Extension of developed test method

The demonstrated test method provides a direct measure of the uniaxial tensile response of UHPFRC, thus facilitating the engagement of these types of concrete in the design of structural components. Specifically, this test method allows for the development of strain-based structural design provisions akin to existing provisions for other common structural materials. Additionally, this test method facilitates the systematic, nonbiased assessment of critical UHPFRC mechanical properties by allowing for independent quality assurance testing of the concrete. Finally, the applicability of this test method to either cast or extracted specimens allows for the physical assessment of in-place UHPFRC mechanical performance of structures and should allow for future refinement in the understanding of fiber reinforcement performance as related to casting considerations.

CONCLUSIONS

Based on the results of the experimental investigation presented herein, the following conclusions are presented:

1. The developed test method represents a foundation from which a reliable, practical method to directly capture the uniaxial tensile stress-strain response of UHPFRC can be created. The developed test method meets critical test requirements, including the ability to be completed relatively quickly on either cast or extracted specimens through the use of commercially available testing equipment.

2. The use of longer specimens is recommended, as increased specimen length reduces the magnitude of bending stresses imparted during the initial gripping of the specimen.

3. In this test program, the uniaxial tensile response of UHPFRC was observed to include four distinct phases: elastic, multi-cracking, crack straining, and localization. Respectively, these phases correspond to elastic behavior, repeated inelastic cracking of the cementitious matrix,

straining within discrete cracks, and localization at a single crack.

4. By clearly demonstrating the uniaxial tensile stress-strain response of UHPFRC without engaging empirical relationships or sophisticated analyses, the developed test method can serve as a reference for other UHPFRC tensile test methods while also facilitating the creation of strain-based structural design criteria for this concrete.

REFERENCES
1. Richard, P., and Cheyrezy, M., "Composition of Reactive Powder Concretes," *Cement and Concrete Research*, V. 25, No. 7, 1995, pp. 1501-1511.

2. Naaman, A. E., and Reinhardt, H. W., "Characterization of High Performance Fiber Reinforced Cement Composites—HPFRCC," *High Performance Fiber Reinforced Cement Composites 2*, A. E. Naaman and H. W. Reinhardt, eds., E&FN Spon, London, UK, 1996, pp. 1-24.

3. Behloul, M., "Analyse et modélisation du comportement d'un matériau à matrice cimentaire fibrée à ultra hautes performances," PhD thesis, École Normale Supérieure de Cachan, Cachan, France, Dec. 1996, 182 pp. (in French)

4. AFGC-SETRA, "Ultra High Performance Fibre-Reinforced Concretes," Interim Recommendations, SETRA, Bagneux, France, 2002, 152 pp.

5. Chanvillard, G., and Rigaud, S., "Complete Characterization of Tensile Properties of Ductal® UHPFRC According to the French Recommendations," *Proceedings of the 4th International RILEM Workshop on High Performance Fiber Reinforced Cement Composites (HPFRCC4)*, Ann Arbor, MI, June 15-18, 2003, 14 pp.

6. Graybeal, B., "Practical Means for Determination of the Tensile Behavior of Ultra-High Performance Concrete," *Journal of ASTM International*, V. 3, No. 8, Sept. 2006.

7. Walraven, J., "High Performance Fiber Reinforced Concrete: Progress in Knowledge and Design Codes," *Materials and Structures*, V. 42, 2009, pp. 1247-1260.

8. Toutlemonde, F., and Resplendino, J., *Designing and Building with UHPFRC: State of the Art and Development*, Wiley-ISTE, London, UK, 2010, 814 pp.

9. Graybeal, B., "Ultra-High Performance Concrete," *FHWA-HRT-11-038*, U.S. Department of Transportation, Federal Highway Administration, Washington, DC, Mar. 2011, 8 pp.

10. Graybeal, B., "Structural Behavior of Ultra-High Performance Concrete Prestressed I-Girders," *FHWA-HRT-06-115*, U.S. Department of Transportation, Federal Highway Administration, Washington, DC, Aug. 2006, 104 pp.

11. Fischer, G., and Li, V. C., "Effect of Fiber Reinforcement on the Response of Structural Members," *Engineering Fracture Mechanics*, V. 74, No. 1-2, Jan. 2007, pp. 258-272.

12. Sato, Y.; Pansuk, W.; Den Uijl, J. A.; and Walraven, J. C., "Shear Capacity of High Performance Fiber Reinforced Concrete I-Beams," *8th International Symposium on Utilization of High-Strength and High-Performance Concrete*, Tokyo, Japan, Oct. 27-29, 2008, pp. 369-376.

13. Graybeal, B., "Structural Behavior of a Prototype Ultra-High Performance Concrete Pi-Girder," *NTIS Report No. PB2009-115495*, U.S. Department of Transportation, Federal Highway Administration, Washington, DC, Nov. 2009, 145 pp.

14. Baby, F.; Billo, J.; Renaud, J. C.; Massotte, C.; Marchand, P.; and Toutlemonde, F., "Shear Resistance of Ultra High Performance Fibre-Reinforced Concrete I-Beams," *FraMCoS7*, B. H. Oh, O. C. Choi, and L. Chung, eds., Jeju, Korea, May 2010, pp. 1411-1417.

15. Toutlemonde, F.; Foure, B.; Sorelli, L.; Baby, F.; Marchand, P.; and Ulm, F. J., "An Overview of Research Advances from 2002 Concerning UHPFRC, in View of Updating AFGC Recommendations," *Proceedings of the International Workshop UHPFRC'2009*, Marseille, France, 2010, 17 pp.

16. Bertram, G., and Hegger, J., "Pretensioned UHPC Beams with and without Openings," *Proceedings of 3rd fib International Congress*, Washington, DC, May 2010, 10 pp.

17. ASTM C39/C39M-10, "Standard Test Methods for Compressive Strength of Cylindrical Concrete Specimens," ASTM International, West Conshohocken, PA, 2010, 7 pp.

18. ASTM E8/E8M-09, "Standard Test Methods for Tension Testing of Metallic Materials," ASTM International, West Conshohocken, PA, 2009, 27 pp.

19. RILEM TC-162 TDF, "Final Recommendation of RILEM TC 162-TDF: Test and Design Methods for Steel Fibre Reinforced Concrete Sigma-Epsilon-Design Method," *Materials and Structures*, V. 36, No. 262, 2003, pp. 560-567.

20. ASTM C1609/C1609M-10, "Standard Test Method for Flexural Performance of Fiber-Reinforced Concrete (Using Beam With Third-Point Loading)," ASTM International, West Conshohocken, PA, 2010, 9 pp.

21. Lappa, E., "High Strength Fiber Reinforced Concrete: Static and Fatigue in Bending," PhD dissertation, Delft University of Technology, Delft, the Netherlands, 2007, 220 pp.

22. Wille, K., and Parra-Montesinos, G. J., "Effect of Beam Size, Casting Method and Support Conditions on the Flexural Behavior of Ultra-High Performance Fiber Reinforced Concrete," *ACI Materials Journal*, V. 109, No. 3, May-June 2012, pp. 379-388.

23. Gonnerman, H., and Shuman, E., "Compression, Flexural and Tension Tests of Plain Concrete," *ASTM Proceedings*, V. 28, 1928, pp. 527-564.

24. United States Department of Interior, Bureau of Reclamation, "Procedure for Direct Tensile Strength, Static Modulus of Elasticity, and Poisson's Ratio of Cylindrical Concrete Specimens in Tension," *USBR 4914*, 1992, pp. 726-731.

25. RILEM TC 162-TDF, "Test and Design Methods for Steel Fibre Reinforced Concrete—Recommendations: Uni-Axial Tension Test for Steel Fibre Reinforced Concrete," *Materials and Structures*, V. 34, Jan.-Feb. 2001, pp. 3-6.

26. Wang, Y.; Li, V. C.; and Backer, S., "Experimental Determination of Tensile Behavior of Fiber Reinforced Concrete," *ACI Materials Journal*, V. 87, No. 5, Sept.-Oct. 1990, pp. 461-468.

27. Casanova, P., and Rossi, P., "Analysis and Design of Steel Fibre Reinforced Concrete Beams," *ACI Structural Journal*, V. 94, No. 5, Sept.-Oct. 1997, pp. 595-602.

28. Rossi, P., "High Performance Multimodal Fiber Reinforced Cement Composites (HPMFRCC): The LCPC Experience," *ACI Materials Journal*, V. 94, No. 6, Nov.-Dec. 1997, pp. 478-483.

29. Zhang, J.; Stang, H.; and Li, V., "Experimental Study on Crack Bridging in FRC under Uniaxial Fatigue Tension," *Journal of Materials in Civil Engineering*, ASCE, V. 12, No. 1, Feb. 2000, pp. 66-73.

30. Zheng, W.; Kwan, A. K. H.; and Lee, P. K. K., "Direct Tension Test of Concrete," *ACI Materials Journal*, V. 98, No. 1, Jan.-Feb. 2001, pp. 63-71.

31. Roth, M.; Eamon, C. D.; Slawson, T. R.; Tonyan, T. D.; and Dubey, A., "Ultra-High Strength, Glass Fiber-Reinforced Concrete: Mechanical Behavior and Numerical Modeling," *ACI Materials Journal*, V. 107, No. 2, Mar.-Apr. 2010, pp. 185-194.

32. Graybeal, B. A., "Material Property Characterization of Ultra-High Performance Concrete," *FHWA-HRT-06-103*, Federal Highway Administration, Washington, DC, Aug. 2006, 186 pp.

33. Morris, A. D., and Garrett, G. G., "A Comparative Study of the Static and Fatigue Behavior of Plain and Steel Fibre Reinforced Mortar in Compression and Direct Tension," *International Journal of Cement Composites and Lightweight Concrete*, V. 3, No. 2, 1981, pp. 73-91.

34. Saito, M., and Imai, S., "Direct Tensile Fatigue of Concrete by the Use of Friction Grips," *ACI Journal*, V. 80, No. 5, Sept.-Oct. 1983, pp. 431-438.

35. Dwarakanath, H. V., and Nagaraj, T. S., "Comparative Study of Predictions of Flexural Strength of Steel Fiber Concrete," *ACI Structural Journal*, V. 88, No. 6, Nov.-Dec. 1991, pp. 714-720.

36. Phillips, D. C., and Zhang, B. S., "Direct Tension Test on Notched and Unnotched Plain Concrete Specimens," *Magazine of Concrete Research*, V. 45, No. 162, 1993, pp. 25-35.

37. Boulay, C.; Rossi, P.; and Tailhan, J.-L., "Uniaxial Tensile Test on a New Cement Composite Having a Hardening Behaviour," *Fiber Reinforced Concretes—BEFIB 2004, Proceedings of the Sixth International RILEM Symposium*, Varenna, Italy, 2004, pp. 61-68.

38. Tailhan, J.-L.; Rossi, P.; and Parant, E., "Inverse Numerical Approach to Determine the Uniaxial Tensile Behaviour of a Stress Hardening Cement Composite from Its Bending Behaviour," *Fiber Reinforced Concretes—BEFIB 2004, Proceedings of the Sixth International RILEM Symposium*, Varenna, Italy, 2004, pp. 913-922.

39. Jungwirth, J., "Zum Tragverhalten von zugbeanspruchten Bauteilen aus Ultra-Hochleistungs-Faserbeton," Thesis No. 3429, École Polytechnique Fédérale de Lausanne (EPFL), Lausanne, Switzerland, 2006, 214 pp. (in German)

40. JSCE, "Recommendations for Design and Construction of High Performance Fiber Reinforced Cement Composites with Multiple Fine Cracks," Concrete Engineering Series 82, Japan Society of Civil Engineers, Mar. 2008, 112 pp.

41. Wille, K.; Kim, D. J.; and Naaman, A. E., "Strain-Hardening UHP-FRC with Low Fiber Contents," *Materials and Structures*, V. 44, No. 3, Aug. 2010, 16 pp.

42. Gopalaratnam, V., and Shah, S., "Softening Response of Plain Concrete in Direct Tension," *ACI Journal*, V. 82, No. 3, May-June 1985, pp. 310-323.

43. Kosa, K., and Naaman, A. E., "Corrosion of Steel Fiber Reinforced Concrete," *ACI Materials Journal*, V. 87, No. 1, Jan.-Feb. 1990, pp. 27-37.

44. Li, Z.; Kulkarni, S. M.; and Shah, S. P., "New Test Method for Obtaining Softening Response of Unnotched Concrete Specimen under Uniaxial Tension," *Experimental Mechanics*, V. 33, 1993, pp. 181-188.

45. Graybeal, B., "Simultaneous Structural and Environmental Loading of an Ultra-High Performance Concrete Component," NTIS *Report* No. PB2010-110331, July 2010, 42 pp.

46. Baby, F., "Contribution à l'identification et la prise en compte du BFUP à l'échelle de la structure (Contribution to Identification of UHPFRC Tensile Constitutive Behavior and Accounting for Structural Design)," dissertation, Paris-Est University, Paris, France, Mar. 2012, 512 pp. (in French)

47. Baby, F.; Graybeal, B.; Marchand, P.; and Toutlemonde, F., "A Proposed Flexural Test Method and Associated Inverse Analysis for UHPFRC," *ACI Materials Journal*, V. 109, No. 5, Sept.-Oct. 2012, pp. 545-555.

48. ASTM C469/C469M-10, "Standard Test Method for Static Modulus of Elasticity and Poisson's Ratio of Concrete in Compression," ASTM International, West Conshohocken, PA, 2010, 5 pp.

49. Graybeal, B., "Compressive Behavior of Ultra-High Performance Fiber-Reinforced Concrete," *ACI Materials Journal*, V. 104, No. 2, Mar.-Apr. 2007, pp. 146-152.

50. Reineck, K. H., and Frettlöhr, B., "Tests on Scale Effect of UHPFRC under Bending and Axial Forces," *Proceedings of the 3rd fib International Congress*, Washington, DC, May 2010, 14 pp.

51. Meade, T., and Graybeal, B., "Flexural Response of Lightly Reinforced Ultra-High Performance Concrete Beams," *Proceedings of the 3rd fib International Congress*, Washington, DC, May 2010, 17 pp.

52. Kabele, P., "Multiscale Framework for Modeling of Fracture in High Performance Fiber Reinforced Cementitious Composites," *Engineering Fracture Mechanics*, V. 74, 2007, pp. 194-209.